Journal of The Electrochemical Society, **158** (11) P123-P129 (2011)
0013-4651/2011/158(11)/P123/7/$28.00 © The Electrochemical Society

Diffusion Barrier Characteristics of Electroless Co(W,P) Thin Films to Lead-Free SnAgCu Solder

Hung-Chun Pan and Tsung-Eong Hsieh[z]

Department of Materials Science and Engineering, National Chiao Tung University, Hsinchu, Taiwan 30010

Diffusion barrier and bonding characteristics of amorphous and polycrystalline electroless Co(W,P) layers (α-Co(W,P) and poly-Co(W,P)) to SnAgCu (SAC) solder were investigated. In the SAC/α-Co(W,P) sample subjected to liquid-state aging at 250°C, the spallation of intermetallic compound (IMC) into solder, a nano-crystalline P-rich layer at SAC/Co(W,P) interface, and the recrystallized Co(W,P) containing Co_2P precipitates were observed. As to the SAC/α-Co(W,P) sample subjected to solid-state aging at 150°C, a thick IMC layer neighboring to the P-rich layer formed at the solder/Co(W,P) interface. Liquid-state aging resulted in an IMC mixture without spallation whereas solid-state aging induced a layer-like IMC in SAC/poly-Co(W,P) samples. Amorphous W-rich layers were also observed in SAC/poly-Co(W,P) samples and it could not inhibit subsequent alloy reactions in the samples. Analytical results indicated the α-Co(W,P) is a sacrificial- plus stuffed-type barrier whereas the poly-Co(W,P) is mainly a sacrificial barrier. The activation energies of IMC growth were 110.7 and 81.8 kJ/mol for SAC/α-Co(W,P) and SAC/poly-Co(W,P) samples, respectively. High P content in α-Co(W,P) was found to degrade the bonding strength to the solder as revealed by the shear test and the control of P content would be a key issue for electroless plating layer applied to under bump metallurgy as the diffusion barrier.
© 2011 The Electrochemical Society. [DOI: 10.1149/2.004111jes] All rights reserved.

Manuscript submitted April 25, 2011; revised manuscript received July 29, 2011. Published October 5, 2011.

At present, development of lead (Pb)-free solders is an important issue in electronic industry due to the call for eliminating Pb to avoid the environment contamination and human damage. In addition to exploring the solders with new constitutions, it is equally important to accumulate the knowledge of materials compatible to practical usages of Pb-free solders. For instance, the flip-chip bonding, a popular interconnection method for advanced electronic packaging which connects the integrated circuit (IC) chips directly to the substrate in a face-down manner, requires the under bump metallurgy (UBM) to facilitate its operation. The UBM mainly serves as the diffusion barrier in between bump body and bond pad material of IC to prevent the degradation resulted from undesired material reactions. As the Pb-free solders may be implanted in the bump body of FC bonding, their interactions with the underlying diffusion barrier materials have to be investigated in detail so as to realize the applications of such solders in electronic products.

Refractory and noble metals, e.g., tungsten (W), molybdenum (Mo), platinum (Pt), palladium (Pd) and rhodium (Rh), are common diffusion barriers for conventional UBM. In contrast to these metallic thin films prepared by sputtering or e-beam evaporation, recently electroless plating layers become a competitive candidate for diffusion barriers since they offer the advantages of low cost, high process throughput, high corrosion resistance and good step coverage. For instance, the lower stress status[1] and better diffusion barrier feature have been reported for electroless nickel (EN) in comparison with the sputtered Ni.[2–5] Further, electroless cobalt-phosphorus (Co(P)) layer was found to possess a good barrier capability in between Cu and interlayer dielectric.[6] Incorporation of W in electroless Co(P), i.e., Co(W,P), might further improve the thermal stability and barrier capability to Cu metallization.[7,8] Feasibility of electroless Co(P) and Co(W,P) to the diffusion barrier to PbSn solder was also reported.[9,10]

The researches regarding of the available barrier materials and Pb-free solders, e.g., the interactions of Ni-base barriers and Pb-free solders,[11–21] are rather flourishing in recent years. However, the diffusion barrier characteristics of electroless Co(W,P) to Pb-free solders are less investigated. This work presents a study on the diffusion barrier characteristics of electroless Co(W,P) to SnAgCu (SAC), the most popular Pb-free solder type. The evolutions of microstructure at the solder/Co(W,P) reacting interfaces were examined in order to gain an understanding on the kinetics of intermetallic compound (IMC) growth. According to these findings, the effects of crystallinity and composition of Co(W,P) on the barrier characteristics are discussed so as to clarify the applicability of electroless Co(W,P) as a barrier material in flip-chip Cu-ICs.

Experimental

Silicon (Si) wafers coated by a 50-nm-thick titanium (Ti) adhesion layer and 100-nm-thick Cu layer to simulate the Cu interconnects were the substrates of this work. The substrates were subjected to a pretreatment listed in Table I and then transferred to a plating bath with constitution and conditions listed in Table II to deposit the electroless Co(W,P) layer with the thickness about 6 to 8 μm.[10] In order to investigate the crystallinity effects on the barrier performance, amorphous and polycrystalline Co(W,P) (termed α-Co(W,P) and poly-Co(W,P) hereafter) were prepared by adjusting the pH value of plating bath within a KOH solution. The α-Co(W,P) prepared at pH = 8.6 contains about 9 to 10 at.% of P and 0.4 to 0.9 at.% of W, whereas the poly-Co(W,P) prepared at pH = 7.6 contains about 4 at.% of P and 8 at.% of W. Note that 1-liter plating solution with composition listed in Table II was able to achieve about 2-μm-thick α-Co(W,P) or 3-μm-thick poly-Co(W,P) layer in 2.5 h. During electroless plating, the pH value of bath was constantly monitored by a pH meter and the plating solution was regularly refurnished so as to yield the electroless layers with desired compositions and film quality. Feasibility of plating process was verified by the microstructure and composition characterizations of samples presented as follows.

After the electroless plating, the eutectic SAC solder paste, Sn-3.0 wt.% Ag-0.5 wt.% Cu (Shenmao Technology Inc., PF606-P, Lot no.:D0806083; melting point = 217 to 219°C;), was immediately applied on the Co(W,P) and a brief reflow in N_2 ambient at 250°C for 30 s was performed to solidify the solder. The samples were annealed in N_2 atmosphere at 250°C up to 5 h for the liquid-state aging or were vacuum-sealed and then subjected to a solid-state aging at 150°C up to 1000 h. Solid-state aging at 130 to 170°C for at least 500 h was also performed to determine the activation energy (E_a) of IMC growth. Scanning electron microscopy (SEM, JSM-6500F) and transmission electron microscopy (TEM, Philips Tecnai F-20) in conjunction with the energy dispersive spectroscopy (EDS, Genesis) were adopted to examine the evolutions of microstructure and compositions in the specimens. The cross-sectional TEM (XTEM) samples were prepared by the focused-ion-beam (FIB, FEI-201) technique supported by Materials Analysis Technology, Inc. at Chupei, Taiwan, R.O.C.

As to the samples for shear test, a Si substrate coated with Ti(50-nm-thick)/Cu(100-nm-thick)/electroless Co(W,P)(about 6 to

[z] E-mail: tehsieh@mail.nctu.edu.tw

Downloaded on 2014-04-24 to IP 140.113.38.11 address. Redistribution subject to ECS terms of use (see ecsdl.org/site/terms_use) unless CC License in place (see abstract).

Table I. Chemicals and processing conditions of pretreatment.[10]

Step	Component	Concentration	Immersion Time
Roughening	H_2SO_4	5 wt.%	30 s
Sensitization	$SnCl_2 \cdot 2H_2O$	10 g/L	5 min
	HCl	40 ml/L	
Activation	$PdCl_2 \cdot 2H_2O$	0.1 g/L	1 min
	HCl	8 ml/L	

8 μm) layers was prepared as mentioned above. A grid pattern of bond pads with 200 μm in diameter were then formed on Co(W,P) by the photolithography process using an SU-8 permanent photoresist (manufactured by MicroChem Corp.; 5%-weight-loss thermal decomposition temperature = 279°C in air) as the mask layer. After the attachment of the 300-μm-diameter SAC solder balls on the pads, a reflow treatment in N_2 at 250°C for 1, 10, 20, 30 or 60 min was carried out to form the shear test samples containing solder ball joints. Shear test was performed in accord with the JSDEC Standard, JESD22-B117A, by using a Dage 4000 multipurpose bond tester supported by Schmidt Scientific Taiwan, Ltd. at Hsinchu, Taiwan, R.O.C. The shear tool standoff was set at 30 μm from the device planar surface and shear speed was set at 100 μm/s. The values of shear force were deduced from the results of at least 25 bumps for each test condition.

Results and Discussion

SAC/α-Co(W,P) samples.— Liquid-state aging.— Figures 1a–1e present the SEM views of SAC/α-Co(W,P) sample at as-reflow condition and those subjected to liquid-state aging for 20 min, 1 h, 3 h and 5 h. As shown in Fig. 1a, the needle-like $CoSn_3$ and $(Co,Cu)Sn_3$ intermetallic compounds (IMCs) at the SAC/α-Co(W,P) interface and Ag_3Sn IMCs dispersed in the interior of solder were observed in the as-reflow sample. After 20-min aging, the spallation of lath-like IMCs into solder occurred and an about 1.7-μm thick reaction layer formed in between IMCs and Co(W,P) as depicted by Fig. 1b. Figures 1c–1e illustrate almost all IMCs spall away from the reaction layer when the aging time exceeds 1 h and the IMCs coarsen into the irregular spheroid form. This observation supports the argument that the IMC spallation is an interface-energy-driven process.[22]

EDS line scan profiles corresponding to the sample shown in Fig. 1c is given in Fig. 1f and Sn and Cu signals are negligibly observed in the unreacted Co(W,P). This indicates α-Co(W,P) may effectively inhibit the interdiffusion of Sn and Cu elements; however, the formation of IMCs depicted in Figs. 1a–1e implies the sacrificial barrier behavior of α-Co(W,P).

EDS analysis also revealed the phosphorus (P) and W concentrations in the reaction layer are as high as 18 at.% and 2.5 at.%, respectively. Owing to the limited solid solubility, accumulation of P and W elements at reacting interface occurred when Co was consumed by Sn to form the IMCs. Such a reaction layer is termed P-rich layer hereafter due to its high-P-content feature. In addition to the interfacial energy reduction of IMCs, the high P content might also cause the IMC spallation since it suppresses the solderability as reported previously.[11–16,23,24]

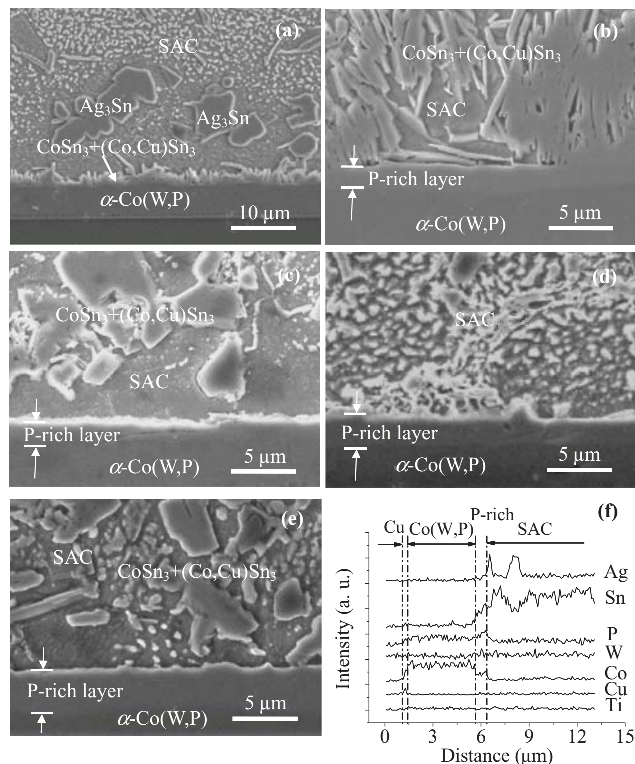

Figure 1. Cross-sectional SEM views of (a) as-reflowed SAC/α-Co(W,P) sample and those subjected to liquid-state aging at 250°C for (b) 20 min, (c) 1 h, (d) 3 h and (e) 5 h. EDS line scan profiles corresponding to (c) is shown in (f).

Figure 2 schematically draws of the thickness of P-rich layer as a function of aging time in log-log scale and the slope of the nearly-straight-line plot was found to be 0.47. This implies the dominance of diffusion-controlled mechanism in the formation of P-rich layer.[21] Previous studies[10,25] and subsequent TEM analysis indicate the P-rich layer is in fact a mixture of nano-scale IMCs. As a result, the diffusion of Sn through P-rich layer to induce the IMC formation at the front of Co(W,P) should be the controlled process. Notably, previous study on eutectic SnBi/Co(W,P) system observed the rates of IMC formation and detachment at the P-rich layer are about the same, leading to a nearly constant value of P-rich layer thickness.[25] In contrast, the P-rich layer apparently thickened with the increase of aging time in the SAC/Co(W,P) system. This is ascribed to a relatively high Sn content

Table II. Chemicals and processing conditions of electroless Co(W,P) plating.[10]

Component		Concentration (g/L)
Co Source	$CoSO_4 \cdot 7H_2O$	23
Reducing Agent	$NaH_2PO_2 \cdot H_2O$	18
Complexing Agent	Na_3 Citrate	144
Buffer Agent	H_3BO_3	31
W Source	$Na_2WO_4 \cdot 2H_2O$	10
pH value		7.6 or 8.6
Temperature		90°C

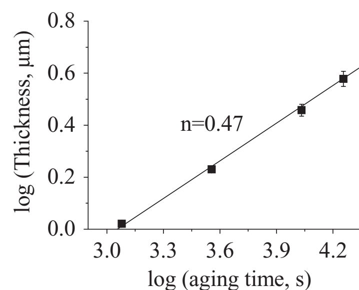

Figure 2. A plot of P-rich layer thickness as a function of aging time for SAC/α-Co(W,P) samples subjected to liquid-state aging test at 250°C in log-log scale. The *n* value represents the slope of linear plot.

Downloaded on 2014-04-24 to IP 140.113.38.11 address. Redistribution subject to ECS terms of use (see ecsdl.org/site/terms_use) unless CC License in place (see abstract).

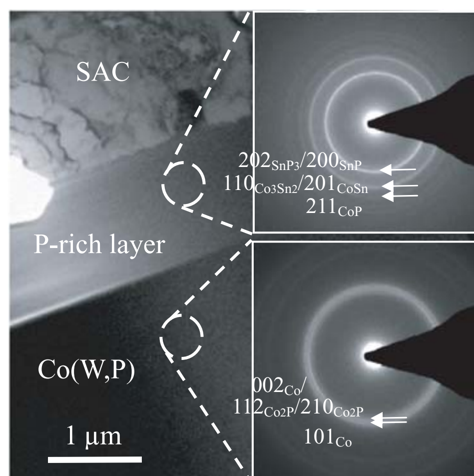

Figure 3. XTEM micrograph of SAC/α-Co(W,P) sample subjected to 1-h liquid-state aging.

in Pb-free SAC solder which results in more Sn flux into the P-rich layer and thus promotes the IMC formation.

The SAC/α-Co(W,P) sample subjected to 1-h liquid-state aging was also characterized by TEM and the result is presented in Fig. 3. Insets at right-hand side of Fig. 3 show the selected area electron diffraction (SAED) patterns taken from the P-rich layer and unreacted Co(W,P) area. Concentric rings in the SAED pattern of P-rich layer indicate the polycrystalline feature and, according to the index of pattern, such a layer is comprised of various IMC types. Further, a carful examination of SAED pattern for unreacted Co(W,P) found the initially amorphous Co(W,P) tends to recrystalize and the cobalt phosphide phase, Co_2P, emerges. The presence of uniformly dispersed Co_2P phase can also be seen in the TEM image of unreacted Co(W,P) as shown in Fig. 3. Since there is a negligible Cu and Sn diffusion into Co(W,P) as revealed by EDS analysis shown in Fig. 1f, it is believed that the supersaturated P content and Co_2P precipitates might provide the stuffed-type barrier capability for α-Co(W,P). Hence, the electroless α-Co(W,P) serves as a combined-type, i.e., sacrificial- plus stuffed-type, barrier in SAC/α-Co(W,P)/Cu system.

Solid-state aging.— Figures 4a–4c present the SEM image, EDS line scan profiles and TEM micrograph of a SAC/α-Co(W,P) sample subjected to solid-state aging at 150°C for 1000 h. As depicted in Fig. 4a, the $(Cu,Co)_6Sn_5$ IMCs agglomerate at the reacting interface without spalling into the solder due to the solid reacting environment. Absence of Cu and Sn signals in unreacted Co(W,P) revealed by EDS line scan shown in Fig. 4b delineate the barrier capability of Co(W,P). Above results illustrate the sacrificial-type barrier feature of α-Co(W,P), similar to that reported in the liquid-state-aging experiment. Formation of polycrystalline P-rich layer was also observed by TEM as shown by the SAED inset at upper left-hand corner of Fig. 4c. The emergence of bright spots randomly embedded in SAED patterns is ascribed to the relatively long solid-state aging time which results in the coarsening of IMCs in P-rich layer. Further, the TEM image contrast also reveals a fine dispersion of nano-scale precipitates in unreacted Co(W,P) and, in conjunction with SAED analysis, they should be the phosphide phase formed due to the supersaturated P elements in α-Co(W,P). Hence, the analytical results regarding of the solid-state aged sample also indicate the combined-type barrier behavior for α-Co(W,P), similar to that reported in previous section.

SAC/Poly-Co(W,P) samples.— *Liquid-state aging.*— Figures 5a–5c present the SEM image, EDS line scan profiles and TEM micrograph of SAC/poly-Co(W,P) sample subjected to the liquid-state aging at 250°C for 1 h. EDS analysis revealed the $CoSn_3$ is the main IMC type while $(Co,Cu)Sn_3$ and $(Co,Ag)Sn_3$ IMCs are occasionally

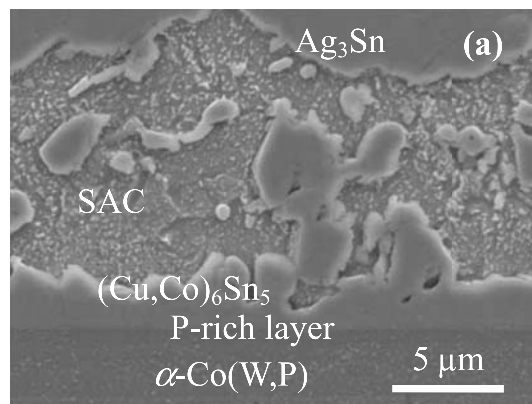

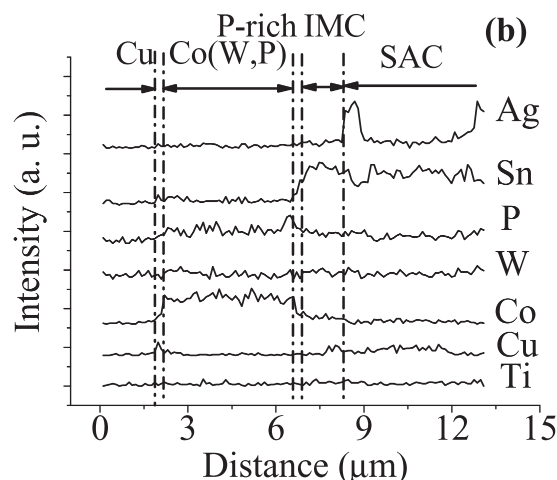

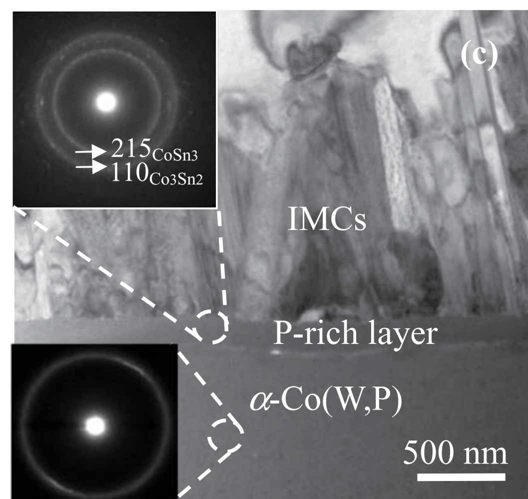

Figure 4. (a) SEM image, (b) EDS line scan profiles and (c) XTEM micrograph of SAC/α-Co(W,P) sample subjected to solid-state aging at 150°C for 1000 h.

observed. In contrast to the α-Co(W,P) sample subjected to liquid-state aging, IMCs do not spall away from the reacting interface in the poly-Co(W,P) system (see Figs. 5a and 5c) and the IMC layer apparently thickens with the increase of aging time as indicated Fig. 6 which plots the IMC thickness as a function of aging time. Note that the slope of plot in Fig. 6 deduced by the linear curve fitting method is about 0.56. The slope close to 0.5 implies the IMC thickening is *via* a diffusion-controlled process, i.e., the diffusion of Sn through presenting IMC to react with Co underlayer. The liquid-solid interactions

Downloaded on 2014-04-24 to IP 140.113.38.11 address. Redistribution subject to ECS terms of use (see ecsdl.org/site/terms_use) unless CC License in place (see abstract).

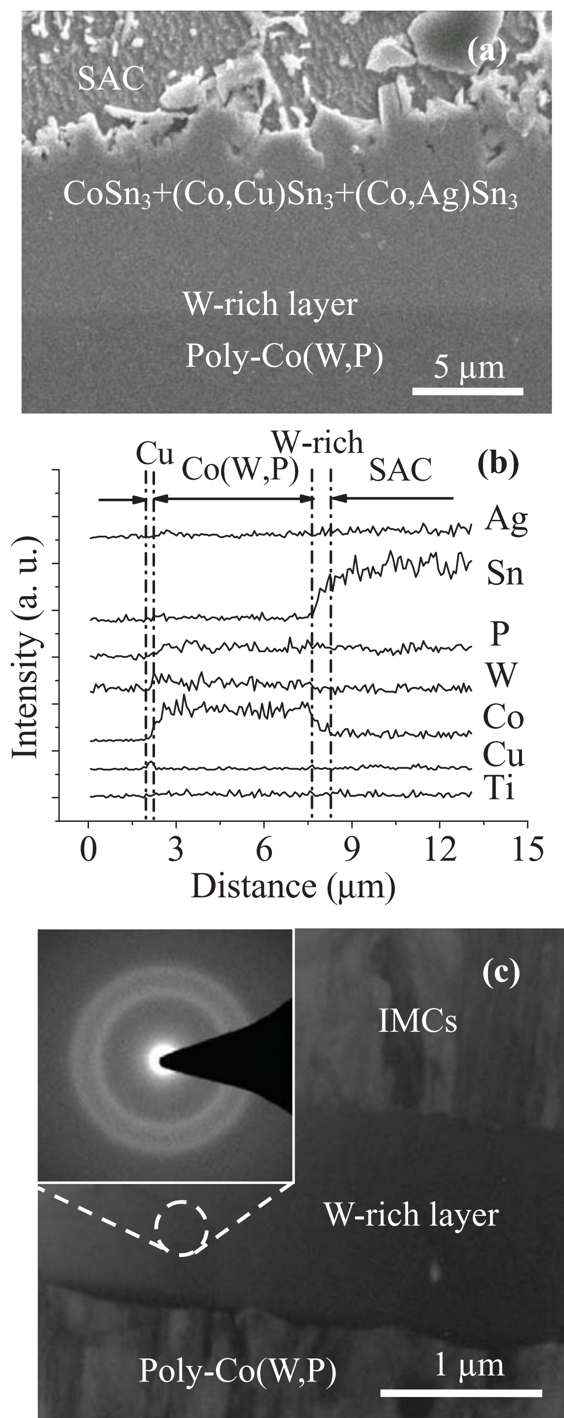

Figure 5. (a) SEM image, (b) EDS line scan profiles and (c) XTEM micrograph of SAC/poly-Co(W,P) sample subjected to liquid-state aging at 250°C for 1 h.

at the molten solder-IMC interface would be less significant in IMC formation although the sample was subjected to the liquid-state aging.

TEM/EDS analysis revealed a distinctive feature in the poly-Co(W,P) sample that an amorphous layer enriched with W elements (∼13.5 at.%; termed W-rich layer hereafter) emerges in beneath the IMCs as depicted by the XTEM micrograph shown in Fig. 5c. The exceptionally high W content is ascribed to the element accumulation during the reaction of Sn and Co as well as the comparatively low P content in poly-Co(W,P). Notably, the plot of Fig. 6 delineates the amorphous W-rich layer does not inhibit subsequent alloy reactions

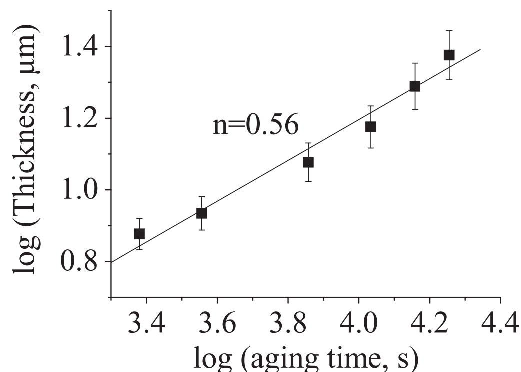

Figure 6. A plot of IMC thickness as a function of aging time for SAC/poly-Co(W,P) samples subjected to liquid-state aging at 250°C in a log-log scale. The *n* value represents the slope of linear plot.

of Sn and Co to form IMCs. Hence, the barrier capability is correlated to the nature of chemical bonds of the interacting materials[25] rather than the structure amorphism of the barrier layer as proposed by conventional classification scheme.[26]

Solid-state aging.— SEM image, EDS line scan profiles, and XTEM micrograph of SAC/poly-Co(W,P) sample subjected to the solid-state aging at 150°C for 1000 h are separately presented in Figs. 7a–7c. A smoother IMC layer mainly constituted by the $(Cu,Co)_6Sn_5$ and a thinner W-rich layer were observed in the SAC/poly-Co(W,P) sample subjected to the solid-state aging, a result of the solid reacting environment and lower temperature of solid-state aging. In conjunction with the analytical results presented in the case of liquid-state aging, the electroless poly-Co(W,P) is categorized as a sacrificial-type diffusion barrier. Poly-Co(W,P) might also possess the stuffed-type barrier feature since the P elements may segregate to the grain boundaries of polycrystalline layer to block the atomic diffusion. However, such a behavior is less obvious in poly-Co(W,P) due to its lower P content in comparison with the case of α-Co(W,P). As a matter of fact, a pronounced IMC growth depicted by Fig. 6 clearly illustrates the dominance of sacrificial-type barrier feature in poly-Co(W,P).

Determination of the E_a of IMC growth.— In this work, the IMC thickness data as a function of time in the samples containing α-Co(W,P) and ploy-Co(W,P) subjected to solid-state aging at 130, 150 and 170°C up to 500 h were collected in order to determine the E_a's of IMC growth. For the purpose of comparison, the sample formed by applying SAC on pure Co metal foil was also prepared for aging test. Figure 8a plots the IMC thickness against the square root of time for various types of samples. At the same aging temperature, the IMC growth rates of SAC/electroless Co(W,P) samples are apparently slower than that of SAC/pure Co sample, evidencing the incorporation of P and W elements suppresses the Co-Sn alloy reactions and thus benefits the barrier capability. Further, the linearity of these plots implies the diffusion-controlled IMC growth in the analytical time span and, hence, the IMC thickness-time relation can be expressed by the formula[27–29]

$$x = \sqrt{Kt} \quad [1]$$

where x is thickness of IMC, t is aging time duration and K is constant correlating to the diffusional growth of IMC. The values of K can be determined from the slopes of plots presented in Fig. 8a and it is known that K can be expressed in the Arrhenius form:

$$K = A \exp\left(-\frac{E_a}{RT}\right) \quad [2]$$

where A is constant, E_a is activation energy for IMC growth, R is ideal gas constant and T is absolute temperature. The values of E_a were calibrated from the slopes of ln$K$ *versus* 1/T plotted in Fig. 8b,

Downloaded on 2014-04-24 to IP 140.113.38.11 address. Redistribution subject to ECS terms of use (see ecsdl.org/site/terms_use) unless CC License in place (see abstract).

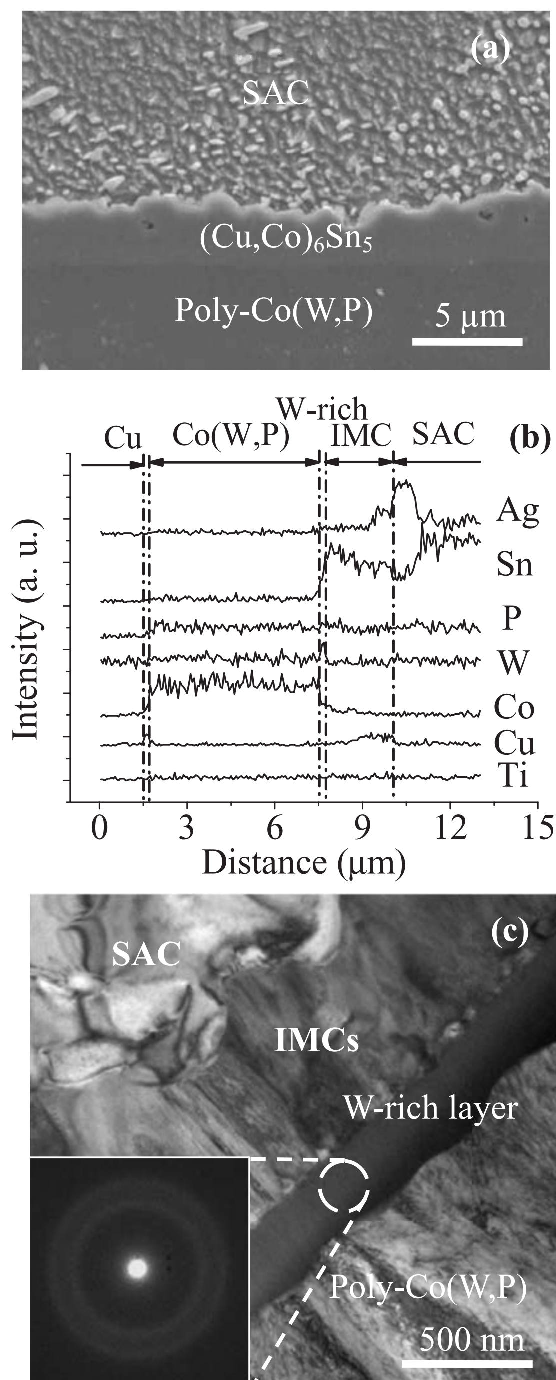

Figure 7. (a) SEM image (b) EDS line scan profiles and (c) XTEM micrograph of SAC/poly-Co(W,P) sample subjected to solid-state aging at 150°C for 1000 h.

and it was found that $E_a = 68$, 81.8, and 110.7 kJ/mole for pure Co, electroless poly-Co(W,P), and electroless α-Co(W,P), respectively. Apparently, the relatively high P and W contents leading to the stuffed-type characteristic enhances the barrier capability of α-Co(W,P) so that it becomes a more efficient diffusion barrier. Here the improvement of barrier capability is not ascribed to the amorphism of α-Co(W,P) since previous TEM characterization has illustrated that the structure amorphism is unnecessarily correlated to the barrier capability of materials.

Shear test.— Figure 9 depicts the average shear strengths of SAC/α-Co(W,P) and SAC/poly-Co(W,P) samples as a function of

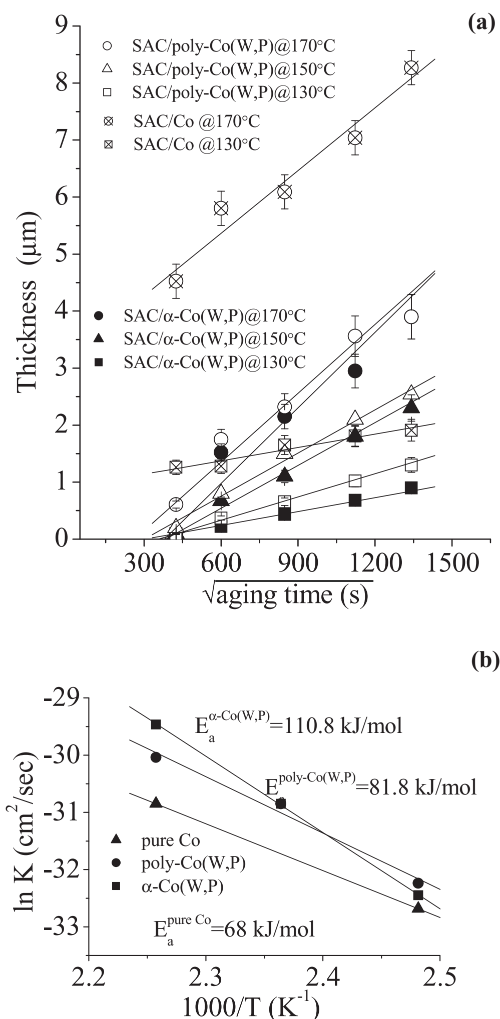

Figure 8. (a) IMC thickness against the square root of time for various SAC/Co samples subjected to solid-state aging at 130–170°C up to 500 h. (b) Plots of ln$K$ *versus* 1/T for the determination of the values of E_a for IMC growth.

time of liquid-state aging. Experimental results of SAC/electroless α-Ni(P)[19,20] and SAC/electrolytic Ni/Au[21] systems are also attached in Fig. 9 for comparison. It can be seen that, regardless of crystallinity of Co(W,P), the SAC/Co(W,P) systems exhibit rather high shear strengths in comparison with the systems utilizing Ni as the barrier layers. For SAC/α-Co(W,P) sample, the shear strength increased from 62.3 MPa to 91.6 MPa after 10-min aging. The bonding strength increased slightly when ageing time was raised to 30 min and then dropped to 80.8 MPa after 1-h aging. Suppression of mechanical strength due to IMC spallation in the FC bonding systems has been reported previously.[30,31] In conjunction with the SEM characterizations presented in Fig. 1, this was similarly observed in the SAC/α-Co(W,P) sample that the bonding strength decreased when a substantial IMC spallation occurred in the 1-h aged sample. In the meantime, the solder became in contact with the P-rich layer with highly accumulated P elements. This led to the deterioration of solderability which, in turn, caused the degradation of bonding strength.

As to the SAC/poly-Co(W,P) sample, a maximum shear strength about 112.8 MPa was observed in 20-min aged sample and there was no drop in bonding strength when aging time extended to 1 h. As illustrated in Fig. 8a which depicts an increase of IMC thickness with the increase of aging time, this is similar to previous studies[21,31–37] which reported the thickening of IMC have no apparent influence on bonding strength. Though bonding strength seems insensitive to the thickness of IMCs, the fracture mode changed in the samples subjected to prolonged aging presented as follows. Furthermore, the P content

Downloaded on 2014-04-24 to IP 140.113.38.11 address. Redistribution subject to ECS terms of use (see ecsdl.org/site/terms_use) unless CC License in place (see abstract).

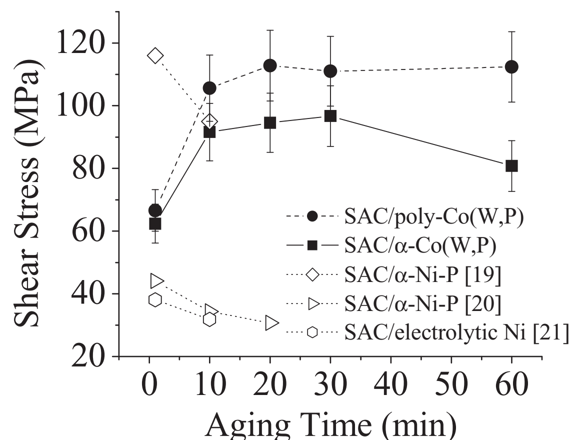

Figure 9. Shear strengths of SAC/Co(W,P) samples as a function of liquid-stage aging time. The results obtained by the studies[19–21] regarding of Ni barrier layers are also added for comparison.

in ploy-Co(W,P) is comparatively lower than that in α-Co(W,P) and there is no IMC spallation in poly-Co(W,P) system as shown in Fig. 5. Analytical results presented above clearly indicate high P content is in fact adverse to the bonding strength. In practical view, the control of P content would be a key issue for electroless plating layer applied to UBM as the diffusion barrier.

Figures 10a and 10b separately present the summary of failure modes for SAC/α-Co(W,P) and SAC/poly-Co(W,P) samples in terms of the SEM observations on fracture surfaces and the JESD22-B117A Standard. As revealed by a representative image of fracture surface shown in Fig. 11a, both as-reflow samples exhibited the interfacial break (mode #4) mode since the exposure of IMC debris indicated the occurrence of fracture at solder/IMC interfaces. When the aging time was increased to about 10 to 20 min, about 20% of α-Co(W,P) samples transformed from interfacial break to ductile mode (mode #1) while all poly-Co(W,P) samples fractured by such a ball shear mode as illustrated by an SEM image shown in Fig. 11b. Emergence of ductile mode indicated the completion of alloy interactions implies a good bonding in between solder and Co(W,P) layer so that the fracture occurs in the bulk of bumps. Pad lift (mode #2) dominated the fracture mode in α-Co(W,P) samples subjected to the aging for more than 20 min as shown by Fig. 10a. The pad lift behavior is depicted by a typical fracture surface image in Fig. 11c which reveals the removal of Co(W,P) layer with solder ball to expose the Cu underlayer. We note the cracked Co(W,P) layers were occasionally observed in α-Co(W,P) samples subjected to prolonged aging as shown in Fig. 11d. In addition to the brittle features of IMCs[38–40] and deterioration of adhesion due to the high P content, the pad lift behavior might also be correlated to the formation of Co_2P precipitates and the glassy transition of α-Co(W,P) layer. The precipitation hardening increases the hardness and suppresses the toughness of α-Co(W,P) layer. The amorphous-to-crystalline transition in aged Co(W,P) layer caused a change of thermal expansion coefficient (CTE) which, in turn, induced the thermal stress that might break the barrier layer. Delamination and, hence, the pad lift occurred to degrade the bonding strength of α-Co(W,P) samples subjected to prolonged aging. This might be a weakness for amorphous-type diffusion barrier when exposed to high-temperature environments in practical applications.

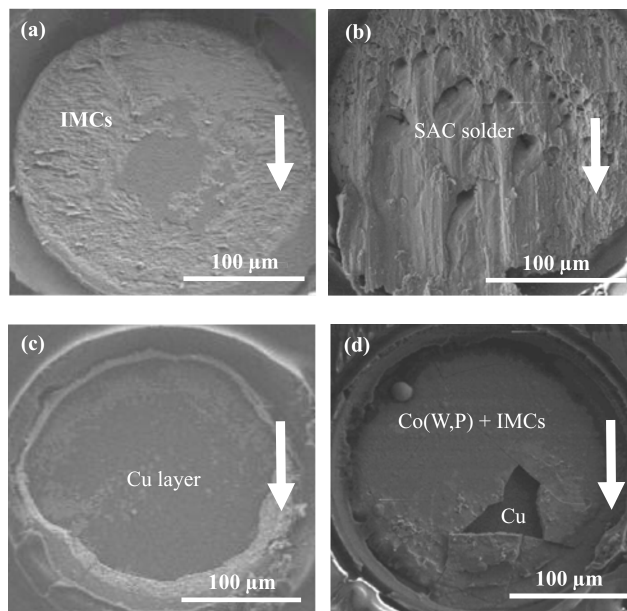

Figure 11. Fracture surfaces of (a) as-reflow SAC/poly-Co(W,P) sample, (b) SAC/poly-Co(W,P) sample subjected to 20-min aging, (c) SAC/α-Co(W,P) sample subjected to 20-min aging and (d) crack of Co(W,P) layer in SAC/α-Co(W,P) sample subjected to 30-min aging. The arrow in each micrograph indicates the shear direction.

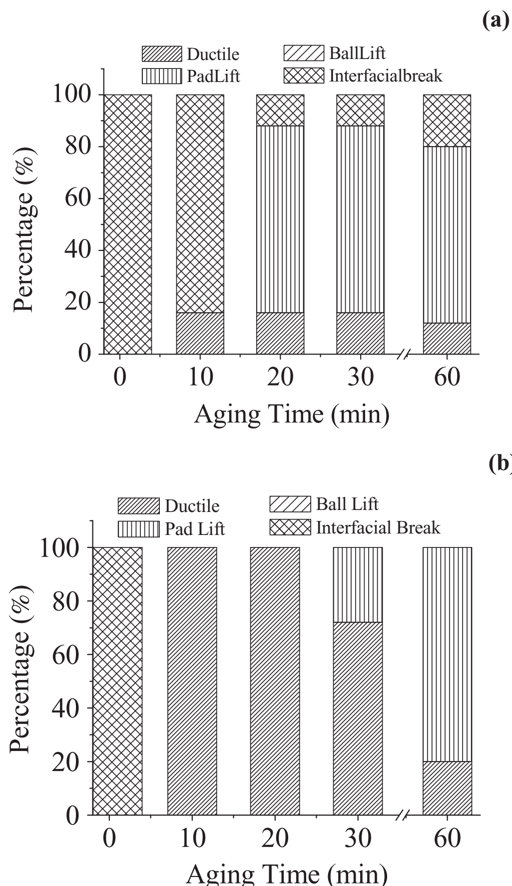

Figure 10. Summary of failure modes of (a) SAC/α-Co(W,P) and (b) SAC/poly-Co(W,P) samples in terms of the SEM observations on facture surfaces and JESD22-B117A Standard.

Ductile mode remained the main fracture mode for poly-Co(W,P) samples subjected to aging up to 30 min. The desired failure mode is ascribed to the relatively low P content and absence of recrystallization in aged poly-Co(W,P) layer. As to the samples aged for 1 h, the pad lift became the dominant failure mode. Though no obvious drop in bonding strength, the breakage in a brittle manner was observed during the shear test in a large portion of 1-h aged poly-Co(W,P) samples. The pad lift behavior might be ascribed to the deterioration of adhesion of

Downloaded on 2014-04-24 to IP 140.113.38.11 address. Redistribution subject to ECS terms of use (see ecsdl.org/site/terms_use) unless CC License in place (see abstract).

electroless Co(W,P) on Cu underlayer; however, the exact origin of this phenomenon is still required further study.

Conclusions

Diffusion barrier characteristics of electroless α-Co(W,P) and poly-Co(W,P) layers to lead-free SAC solder were investigated. In the SAC/α-Co(W,P) sample subjected to the liquid-state aging, $(Co,Cu)Sn_3$ IMC spalled into solder and a nano-crystalline P-rich layer formed in between the SAC and Co(W,P). Further, the aging treatment induces the recrystallization of α-Co(W,P) and precipitation of Co_2P phase. As to the SAC/α-Co(W,P) sample subjected to solder-state aging, a thick $(Cu,Co)_6Sn_5$ IMC formed in between SAC and Co(W,P) without spallation and a P-rich layer beneath the IMCs was similarly seen. Analytical results indicate the α-Co(W,P) is combined-type, i.e., sacrificial- plus stuffed-type, barrier regardless of aging type.

For SAC/poly-Co(W,P) sample subjected to the liquid-state aging test, a mixture of $CoSn_3$, $(Co,Cu)Sn_3$ and $(Co,Ag)Sn_3$ IMC layer neighboring to a thin amorphous W-enriched layer formed in between solder and Co(W,P). As to SAC/poly-Co(W,P) sample subjected to solid-state aging, a smoother $(Cu,Co)_6Sn_5$ IMC layer and a thinner W-rich layer were observed in the reacting interface. Analytical results indicated poly-Co(W,P) is mainly a sacrificial barrier layer. In addition, above characterizations illustrated the diffusion barrier capability should originate from the nature of chemical bonds rather than the amorphism in microstructure.

The values of E_a of IMC growth for SAC/pure Co, SAC/poly-Co(W,P), and SAC/α-Co(W,P) samples deduced from the solid-state aging were found to be 68, 81.8, and 110.7 kJ/mole, respectively. The enhancement of barrier capability in α-Co(W,P) is ascribed to its relatively high P content which leads to the stuffed-type characteristic in the electroless layer.

As indicated by the ball shear test, SAC/α-Co(W,P) and SAC/poly-Co(W,P) samples exhibited bonding strength as high as 91.6 and 112.8 MPa, respectively. In SAC/α-Co(W,P) case, interfacial break was observed at short-time aged samples while pad lift became the dominant failure mode when aging time was long. The decrement of bonding strength due to pad lift failure was ascribed to the deterioration of adhesion due to high P content, loss of toughness due to the formation of Co_2P precipitates and the thermal stress induced by the difference of CTE due to the recrystallization in aged Co(W,P) layer. Except in the as-reflow sample, the ductile mode dominated the failure of SAC/poly-Co(W,P) samples in most aging conditions. The shear test indicated the high P content in α-Co(W,P) is in fact adverse to the mechanical performance of bump joints although it additionally provides the stuffed-type barrier capability to sacrificial barrier feature when implanted in UBM structure.

Acknowledgments

This work is supported by the National Science Council (NSC), Taiwan, R.O.C., under the contract No. NSC-96-2221-E-009-010. The supports of microstructure analysis and XTEM sample preparation by Materials Analysis Technology, Inc., Chupei, Taiwan, R.O.C., is also deeply acknowledged.

References

1. R. H. Uang, K. C. Chen, S. W. Lu, H. T. Hu, and S. H. Huang, in *IEEE Electron. Packaging. Technol. Conf.*, p. 292, Proceedings of 3rd Electronics Packaging Technology Conference (EPTC 2000), Singapore, December 5–7 (2000).
2. M. W. Liang, T. E. Hsieh, C. C. Chen, and Y. T. Hung, *Jpn. J. Appl. Phys.*, **43**, 8258 (2004).
3. T. Oppert, E. Zakel, and T. Teutsch, in *Proc. IEMT / IMC Symp.*, p. 106, 2nd 1998 IEMT/IMC Symposium, Japan, April 15–17 (1998).
4. T. Teutsch, T. Oppert, E. Zakel, and E. Klusmann, in *Electron. Comp. and Technol. Conf.*, p. 107, 2000 Proceedings. 50th Electronic Components and Technology Conference, Las Vegas, NV, Piscataway, NJ USA, May 21–24 (2000).
5. G. O. Mallory and J. B. Hajdu, *Electroless Plating Fundamentals and Applications*, Chap. 1-7, AESF, Orlando, Florida (1990).
6. E. J. O'Sullivan, A. G. Schott, M. Paunovic, C. J. Sambucetti, J. R. Marino, P. J. Bailey, S. Kaja, and K. W. Semkow, *IBM J. Res. Dev.*, **42**, 607 (1998).
7. A. Kohn, M. Eizenberg, Y. Shacham-Diamand, and Y. Sverdlov, *Mater. Sci. Eng. A*, **302**, 18 (2001).
8. A. Kohn, M. Eizenberg, Y. Shacham-Diamand, B. Israel, and Y. Sverdlov, *Microelectron. Eng.*, **55**, 297 (2001).
9. M. W. Liang, H. T. Yen, and T. E. Hsieh, *J. Electron. Mater.*, **35**, 1593 (2006).
10. W. C. Wu, T. E. Hsieh, and H. C. Pan, *J. Electrochem. Soc.*, **155**, D369 (2008).
11. C. E. Ho, R. Y. Tsai, Y. L. Lin, and C. R. Kao, *J. Electron. Mater.*, **31**, 584 (2002).
12. C. W. Hwang and K. Suganuma, *J. Mater. Res.*, **18**, 2540 (2003).
13. Y. C. Lin and J. G. Duh, *Scripta Mater.*, **54**, 1661 (2006).
14. Y. C. Lin, T. Y. Shih, S. K. Tien, and J. G. Duh, *Scripta Mater.*, **56**, 49 (2007).
15. V. Vuorinen, T. Laurila, H. Yu, and J. K. Kivilahti, *J. Appl. Phys.*, **99**, 023530 (2006).
16. Y. C. Lin, J. G. Duh, and B. S. Chiou, *J. Electron. Mater.*, **35**, 7 (2006).
17. Y. C. Lin and J. G. Duh, *J. Electron. Mater.*, **35**, 1665 (2006).
18. Y. C. Lin, T. Y. Shih, S. K. Tien, and J. G. Duh, *J. Electron. Mater.*, **36**, 1469 (2007).
19. D. G. Kim, J. W. Kim, S. S. Ha, B. I. Noh, J. M. Koo, D. W. Park, M. W. Ko, and S. B. Jung, *J. Alloy. Compd.*, **458**, 253 (2008).
20. X. Gu, Y. C. Chan, D. Yang, and B. Y. Wu, *J. Alloy. Compd.*, **468**, 553 (2009).
21. P. Liu, P. Yao, and J. Liu, *J. Alloy. Compd.*, **470**, 188 (2009).
22. C. Y. Liu, H. K. Kim, K. N. Tu, and P. A. Totta, *Appl. Phys. Lett.*, **69**, 4014 (1996).
23. Y. C. Sohn, J. Yu, S. K. Kang, D. Y. Shih, and T. Y. Lee, *J. Mater. Res.*, **19**, 2428 (2004).
24. J. J. Guo, A. P. Xian, and J. K. Shang, *Surf. Coat. Technol.*, **202**, 268 (2007).
25. H. C. Pan and T. E. Hsieh, *J. Electron. Mater.*, **40**, 330 (2011).
26. M. A. Nicolet, *Thin Solid Films*, **52**, 415 (1978).
27. V. I. Dybkov and O. V. Duchenko, *J. Alloy. Compd.*, **234**, 295 (1996).
28. A. Sharif and Y. C. Chen, *Mater. Sci. Eng. B*, **106**, 126 (2004).
29. D. Q. Yu, C. M. L. Wu, C. M. T. Law, L. Wang, and J. K. L. Lai, *J. Alloy. Compd.*, **392**, 192 (2005).
30. C. W. Hwang, K. Suganuma, M. Kiso, and S. Hashimoto, *J. Electron. Mater.*, **33**, 1200 (2004).
31. P. C. Shih and K. L. Lin, *J. Alloy. Compd.*, **422**, 153 (2006).
32. J. W. Yoon, S. W. Kim, and S. B. Jung, *J. Alloy. Compd.*, **385**, 192 (2004).
33. J. W. Yoon, S. W. Kim, and S. B. Jung, *J. Alloy. Compd.*, **391**, 82 (2005).
34. J. W. Yoon, S. W. Kim, and S. B. Jung, *J. Alloy. Compd.*, **392**, 247 (2005).
35. C. T. Lin, C. S. Hsi, M. C. Wang, T. C. Chang, and M. K. Liang, *J. Alloy. Compd.*, **459**, 225 (2008).
36. P. Yao, P. Liu, and J. Liu, *J. Alloy. Compd.*, **462**, 73 (2008).
37. A. K. Gain, T. Fouzder, Y. C. Chan, A. Sharif, and W. K. C. Yung, *J. Alloy. Compd.*, **489**, 678 (2010).
38. H. T. Lee, S. Y. Hu, T. F. Hong, and Y. F. Chen, *J. Electron. Mater.*, **37**, 867 (2008).
39. J. Shen and Y. C. Chan, *J. Alloy. Compd.*, **477**, 552 (2009).
40. S. Y. Chang, Y. C. Huang, and Y. M. Lin, *J. Alloy. Compd.*, **490**, 508 (2010).

Downloaded on 2014-04-24 to IP 140.113.38.11 address. Redistribution subject to ECS terms of use (see ecsdl.org/site/terms_use) unless CC License in place (see abstract).